CFD Study of Pressure Distribution on Recessed Faces of a Diamond C-Shaped Building

Arun Kumar , Rahul Kumar Meena , Ritu Raj , Mohammad Iqbal Khan * , Jamal M. Khatib

Posted Date: 8 October 2023

doi: 10.20944/preprints202310.0443.v1

Keywords: Diamond C- shape Tall Building; Wind Loads; ANSYS (CFX); Pressure Coefficients

Article

CFD Study of Pressure Distribution on Recessed Faces of a Diamond C-Shaped Building

Arun Kumar [1], Rahul Kumar Meena [2], Ritu Raj [1], Mohammad Iqbal Khan [3,*] and Jamal M. Khatib [4]

[1] Department of Civil Engineering, DTU, India arunkumar.dtu@gmail.com (A.K.), rituraj@dtu.ac.in (R.R.)
[2] Department of Civil Engineering, Punjab Engineering College, Chandigarh, India; rahul.08dtu@gmail.com (R.K.M)
[3] Department of Civil Engineering, College of Engineering, King Saud University, P.O. Box 800, Riyadh 11421, Saudi Arabia;
[4] Faculty of Science and Engineering, University of Wolverhampton, Wolverhampton WV1 1LY, UK; j.m.khatib@wlv.ac.uk (J.M.K.)
* Correspondence: miqbal@ksu.edu.sa (M.I.K.)

Abstract: Building situated in the flow path of wind is subjected to differential velocity and pressure distribution around the building envelope. Wind effects are influenced and vary for each individual shape of the tall building. Tall building structures are considered as cantilever structures with fixed ends at the ground. Wind exponential velocity acting along the height of the building makes velocity and pressure distribution more complex as the height of the building structure increases. This study discussed the effect of wind on an irregular cross-section shape. The study was conducted numerically with a building model placed in a virtual wind tunnel using the ANSYS (CFX) software tool. Wind effects are investigated on building model situated in a terrain category - II defined in IS: 875 (Part 3): 2015 wind scale model of 1:100 and turbulence intensity is 5 % and power law index α is considered as 0.143. Validation and verification of the study were made by comparing pressure coefficients on faces of a rectangular model of similar floor area and height as taken for a C-plan diamond-shaped model under similar boundary conditions, wind environment, and solver setting of numerical setup. The values of surface pressures generated on the recessed faces of the model and wind flow patterns within the recessed cavity were studied at wind incident angles 0°, 30^0, 60°, 105^0, 135^0 & 180^0. The critical suction on all the recessed faces was observed to be at a 105° angle of wind attack.

Keywords: diamond C- shape tall building; wind loads; ANSYS (CFX); pressure coefficients

1. Introduction

To fulfill the requirement of housing for all, high-rise building construction has become a necessity, especially in urban and metropolitan cities. It is essential to evaluate wind impact on such high-rise buildings for the safety of the structure and comfort of the users. In its most basic form, wind flow consists of a succession of gusts that vary greatly in amplitude and direction. Strong wind may cause discomfort to the users and damage to the structure. Extreme winds such as hurricanes, cyclones, and tornados can cause extensive damage to buildings due to the heavy load produced by such winds. The shape and size of the building play an important role in modifying wind-produced load on the building. As the height of the building increases (62 m and above) wind load is more pronounced than the seismic load [1]. As such, it is important to study the wind environment on all types of high-rise buildings.

When the wind is motionless, normal air pressure acts everywhere around the building, balancing the load on the building in totality. Pressure changes from point to point on the building's surface as the wind picks up speed. Theoretically, according to Bernoulli's equation, at the stagnation point on the windward face, where velocity becomes zero, maximum pressure is developed. This pressure is equal

to $\frac{1}{2}\rho u^2$, where ρ and u are air density and wind speed respectively. This is known as velocity/impact pressure [2]. Using Bernoulli's equation, pressure differences at a point can be represented as:

$$C_{Pe} = \frac{\Delta P}{\rho u^2/2} \quad (1)$$

Where, C_{Pe} is a dimensionless entity called pressure coefficient and ΔP is the pressure difference between actual pressure at the point, P and the normal atmospheric pressure P_o acting at that point. In the separated flow and wake regions where shear layers and vorticity do exist, Bernoulli's equation does not hold good due to an increase in flow velocity [3]. However, a good prediction of the pressure coefficient can be made by equation (1). In atmospheric boundary layer (ABL) flow where the exponential rise in velocity field along height occurs due to frictional resistance from the surface of the earth, pressure gradient, Coriolis effect, and earth's rotation, defining the velocity field is not an easy task. ABL is the distance from the mean surface of the earth up to which the exponential gradient velocity field exists. It is up to 300 m to 400 m above the mean surface of the earth. So, u is set at a reference height. The greatest velocity at the rooftop of the model was used to calculate all C_{Pe} values in the current investigation. Points corresponding to the highest C_{Pe}, where impact pressure is greatest, can be found in this manner. A larger pressure drop caused by gustiness of wind at any point causes the average pressure distribution over the windward surface to be greater than the impact pressure. The resulting coefficient is mostly unaffected by wind speed and model scale [2]. It is, however, influenced by the form of the building, wind flow direction, terrain roughness, and proximity to other structures [4]. For structural design purposes, we can find C_{Pe} values for regular plan-shaped buildings in different international codes/standards, but the data are available only for orthogonal directions of wind flow. The value of pressure coefficients given in the codes for structural design are on the conservative side and provide uneconomical construction. For various unconventional architectural shapes, nowadays being used by architects, the values of C_{Pe} are either presumed from the codes, which are relatively inaccurate being approximated from the shapes given in codes, or from wind tunnel experiments, which are costly and time consuming. With the invention of complex computational facilities available nowadays, it is possible to know C_{Pe} values on buildings of different architectural shapes.

Baines [5] was the first to demonstrate how wind velocity distribution and fluid pressure affect tall buildings. He demonstrated the isobars of the mean wind pressure on the windward face to be positive and suction pressures on the side faces, lee face, and rooftop of a tall square structure. Researchers have published a number of scientific papers on the subject of wind effects on various shapes of tall buildings. Gomes [6] used CFD modeling to examine how the flow patterns on L and U shape models changed across a wide range of wind incidence angles. The surface pressure distributions were studied in a wind tunnel test. Wind flow in the recessed cavity of an H-shaped tall building using CFD was studied by [7]. investigate the wind induced response and equivalent wind load on super tall buildings using experimental methods and measured pressure on building models [8]. The flow between the cavity and outside of the cavity for different aspect ratio were studied. The flow within the cavity was found to be neither simply a cross-flow nor a stagnation flow. It is reported that the flow pattern was complex within the cavity and dependent upon the height and formation of two circulation vortices inside the cavity. [9] studied L-shape and T-shape models of similar cross-sectional area and height but different limb lengths. They observed that the cross-sectional shapes and limb lengths are crucial for pressure distribution on faces. However, the magnitude of peak pressure and peak suction on the faces largely depends on wind direction. Mean interference of close proximity rectangular buildings placed in L and T plan shaped building were studied by [10] in the wind tunnel for boundary layer wind flow over extended wind angles and a comparison was made with the response of similar buildings in isolation. Interference effects were reported to be influenced by the position and arrangements of models and wind incidence angles. Wind tunnel studies were used to illustrate the aerodynamic properties of several irregular plan shaped tall buildings [11]. Presented a review of wind effects, instruments are not accurate enough to identify wind load parameter in the nonlinear region [12], CFD study on ANSYS (CFX) was carried out at different wind angles on a rectangular model for interference effect due to

Preprints (www.preprints.org) | NOT PEER-REVIEWED | Posted: 8 October 2023 doi:10.20944/preprints202310.0443.v1

another upstream rectangular model similar in plan area by [13].[14] Studied wind effects on tall buildings and observed that the positive wind effects will be on the wind ward side while negative pressure is on the leeward side. They varied aspect ratio of interfering and principal building models gradually from 1:5 to 5:5. Validity of the work was determined by comparing the pressure coefficients on the surfaces of the building in isolation with IS:875 (part-3)-1987. It was revealed that the wind load on the principal building largely depends upon the aspect ratios of the principal and interfering buildings and wind incident angles. Wind pressure variations on the octagonal plan shape building model in isolated and interfering conditions from three square building models placed at different locations at distances between 0.4 to 2 of the height of the octagonal building were studied by using ANSYS (CFX) [15]. Investigated the wind pressure by varying the geometry or exposure condition, [16] investigated the wind effects on super tall buildings using an experimental method, observing that the twisted wind flow will vary the vortex shedding mainly on the wind ward and side faces. [17] A comparison of pressure on the faces and roofs of a square-tall building and a square tall building with a setback of 0.2L at 0.5H was studied by [18] through ANSYS (CFX). The setback roof was found to be subjected to higher pressure than the top of the roof. [19] used ANSYS (CFX) solver to examine the distribution of wind pressure on an E-plan-shape model. According to reports, values of the coefficient of pressure on faces for different element meshing sizes differ from wind tunnel measurements by 17 to 24%. Interference effects on an H-shape building model with similar building models placed at various positions were investigated by [20]. At full blockage suction produced on the main building was found to be higher than other blockage conditions. Modification of wind flow around two plus shape tall building models in close proximity for interference effects was studied in an open circuit wind tunnel by [21]. According to reports, the increase or decrease in wind load on the building façade was dependent on the relative positioning of the building models. In full blockage condition more suction was reported to occur on the gap faces and severe interference effect was reported at half and no blockage.

Not much study of wind effect on C-shape building models has been found in the available literature. Performed the test to investigate the structural behavior of super tall buildings under strong wind effects it was observed that the turbulent intensity and gust factor decreased as the mean wind speed increased [22]. [23] studied C-shape building models of similar plan areas but different heights. They predicted mean pressure coefficients on the faces through experimental as well as numerical analysis. It has been reported that geometry, aspect ratio, and wind flow pattern have a significant influence on pressure variations on faces. The goal of the current study was to determine how wind loads would affect a structure with a diamond C-plan shape building having a 300 sqm plan area and 50 m height (Figure 1 a) by numerical simulation of building model done on ANSYS (CFX) software using standard k-ε turbulent model. C_{Pe} values obtained on the faces were evaluated for 0° to 180° @ 15° wind attack angles. However, a brief description of the wind flow pattern and typical (critical) values of the coefficient of wind pressure on the recessed faces for 0°, 30^0, 60°, 105^0, 135^0 & 180^0 wind attack angles are presented in this paper.

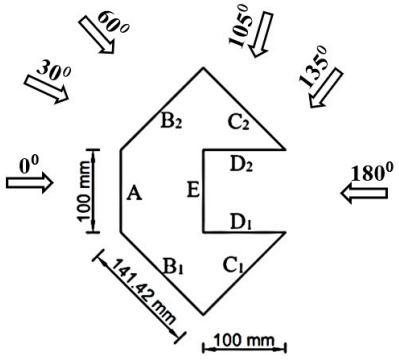

Figure 1. (a): Diamond C-shape Model

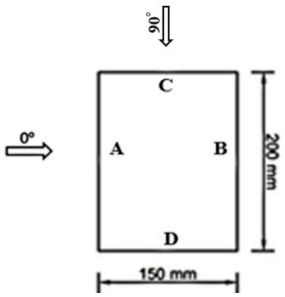

Figure 2. (b): Rectangular Model.

Preprints (www.preprints.org) | NOT PEER-REVIEWED | Posted: 8 October 2023 doi:10.20944/preprints202310.0443.v1

2. Verification and Validation

For validation and verification, a rectangular model (Figure 1 b) of similar floor area and height was simulated under the same wind environment, boundary conditions, and solver setting. Power law was used to apply a homogeneous steady-state wind with 5% turbulence in ABL of the terrain roughness mentioned in the abstract with a roughness coefficient, $\alpha = 0.143$. Free wind velocity and turbulence intensity profile along the height of the building model were plotted and compared with experimental data from [20] and are shown in Figures 2 and 3 respectively. Comparison of the C_{Pe} results on faces of the rectangular model for the two orthogonal directions of wind were compared with that in relevant codes of different countries and for 90° wind angle from experimental data of [24]. The results are presented in Table 1 and are under acceptable limits.

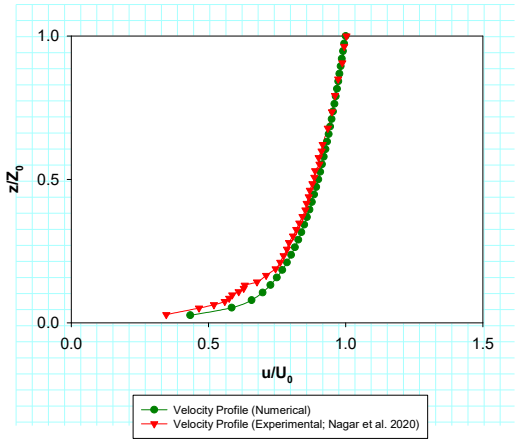

Figure 2. Mean Wind Velocity Profile.

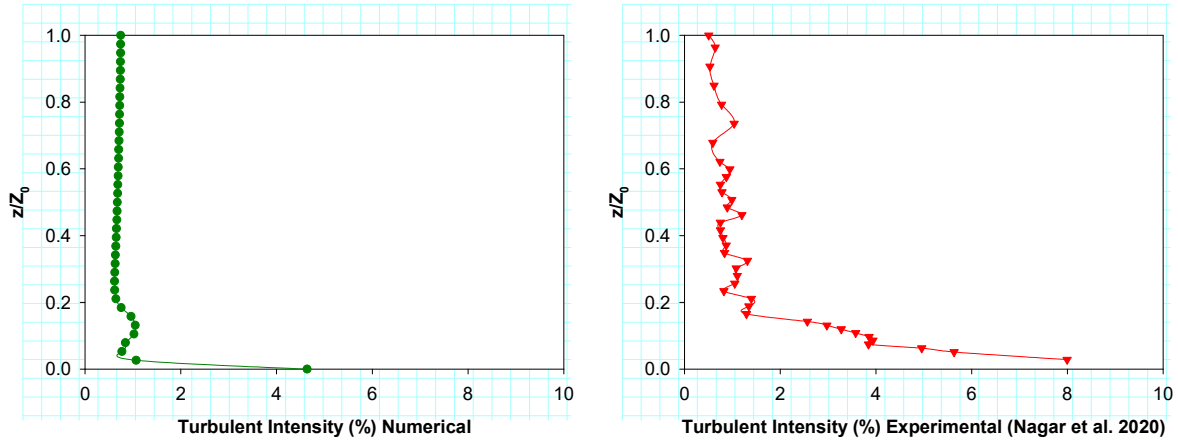

Figure 3. Mean Wind Turbulent Intensity Profile.

Table 1. Comparison of Area Average C_{Pe} on Faces of Rectangular Model.

As per	Wind Angle	C_{Pe} Face A	C_{Pe} Face B	C_{Pe} Face C	C_{Pe} Face D
ANSYX (CFX)	0°	+ 0.70	- 0.28	- 0.60	- 0.60
	90°	-0.60	-0.60	+0.68	-0.27
IS: 875 (Part	0°	+ 0.8	- 0.25	- 0.8	- 0.8
3): 2015	90°	-0.8	-0.8	0.8	-0.25
ASCE/SEI 7-	0°	+ 0.8	- 0.5	- 0.7	- 0.7
10	90°	-0.7	-0.7	0.8	-0.5
	0°	+ 0.8	- 0.5	- 0.65	- 0.65

Preprints (www.preprints.org) | NOT PEER-REVIEWED | Posted: 8 October 2023 doi:10.20944/preprints202310.0443.v1

AS/NZS-1170.2 (2002)	90˚	-0.65	-0.65	0.8	-0.5
EN: 1991-1-4	0˚	0.8	-0.55	-0.8	-0.8
	90˚	-0.8	-08	0.8	-0.55
BS: 6399-2	0˚	0.76	-0.5	-0.8	-0.8
Amin and Ahuja 2013	90˚	-0.8	-0.8	0.76	-0.5
	90˚	-0.66	-0.66	0.74	-0.41

3. Numerical Analysis

Various mathematical models based on Navier-Stokes Equations have been developed by researchers to study the flow simulation of fluids. These models have been presented in the form of differential equations which contains several unknowns and unmeasurable quantity which can be neglected. These differential equations are solved at finite grid locations during simulation. For bluff body wind simulation, the standard k - epsilon $(k-\varepsilon)$ turbulence model is mostly used. It is based on Reynold Averaged Navier-Stokes (RANS) equations in which the continuity and momentum equations are based on the time-averaged steady state velocity of the fluid. It is easy to provide initial and/or boundary conditions in this model. However, it does not predict exactly where high eddies are developed. Nevertheless, the flow pattern and pressure distribution are mapped to a level of acceptable accuracy by introducing additional variables in the form of two transport equations. The one is the production of Turbulence Kinetic Energy (k) due to wind shear and buoyancy and the second is Dissipation of Turbulence Kinetic Energy (ε) due to viscous forces. In ANSYS (CFX) solver theory guide 2012.1 (2009) [25] the equations of continuity and momentum of flow and the two transport equations of turbulence model $(k-\varepsilon)$ are provided on page 57 of the literature.

4. Mean Velocity Characteristics

In nature, as explained earlier in Para 1 that exponential velocity field along height within the ABL zone exists, it is difficult to define velocity load along building height. However, certain equations have been developed for the gradient velocity field in ABL. The power law equation, as described below, is widely used in wind engineering experiments for representing ABL flow.

Power Law:

$$u = u_{Ref}\left(\frac{Z}{Z_{Ref}}\right)^{\alpha} \tag{2}$$

Where, u_{Ref} = Reference wind speed in m/s

Z_{Ref} = Reference height taken as 10 m.

u = Time averaged longitudinal velocity at height Z above ground.

α is the terrain roughness coefficient.

Though this equation is analytically not correct for the bottom 10 m of ABL it provides velocity of wind at higher altitudes well.

5. Computational Domain and Flow Parameter

The wind flow occurring in nature can be represented with good resemblance for the simulation when the computational domain is developed as recommended by [26]. The computational domain was constructed as a parallelopiped large enough in all three directions, with the model placed inside the domain as shown in Figure 4. The precaution was taken to keep the size of the domain large enough so that fluid reflections from the domain walls do not occur and abnormal wind pressure around the model does not happen. Simultaneously, it was ensured that the blockage ratio did not increase above 3%. At the same time, domain size was not kept too large to restrict grid elements within reasonable numbers.

Preprints (www.preprints.org) | NOT PEER-REVIEWED | Posted: 8 October 2023 doi:10.20944/preprints202310.0443.v1

More grid elements require greater computer facilities and more time for convergence of the numerical solution. A model of a Diamond C-shape building with a plan area of 300 sqm and height of 50 m was created with a length scale of 1:100.

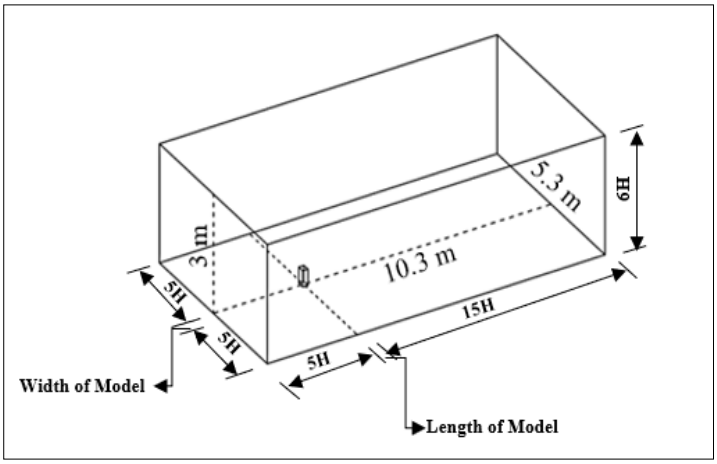

Figure 4. Computational Domain.

6. Computational Grid and Grid Sensitivity

The mesh element size in the domain volume and surface of the model affects the convergence of the solution considerably. The grid resolution was set to precisely capture crucial physical factors of the flow such as pressure on the surface of the model, separation of flow, formation of wake and vortices, reattachment of flow, and so on. Because our primary goal was to measure pressure on the surface of the model, it was discretized into finer elements than the computational domain. The meshing technique for a better solution depends upon the approach to discretize the domain and model surface into smaller elements. In the present study, different regions of the domain were discretized with different element sizes and it was ensured that the solution reaches a steady state. The ratio of element size in the base was varied between 0.50 to 0.40 times the element size of the domain and; model face sizing was varied between 0.25 to 0.2 times the element size of the domain. However, on smaller mesh elements solution took more time. A trade-off among them was adopted. The mesh elements on the model surface were inflated to achieve a smooth transition from the domain elements so that the velocity gradients could be mapped correctly near no-slip walls (Figure 5). Final results were adopted with 0.44 times the element size of the domain on base and 0.22 times on model faces. At this resolution, the solution reached a steady state, and the residual RMS error for mass and momentum convergence was achieved between 10^{-4} to 10^{-5} for momentum in the three directions and up to 10^{-6} for mass respectively. The corresponding domain imbalances in the values were 0.001% for momentum in the three directions and 0% for mass.

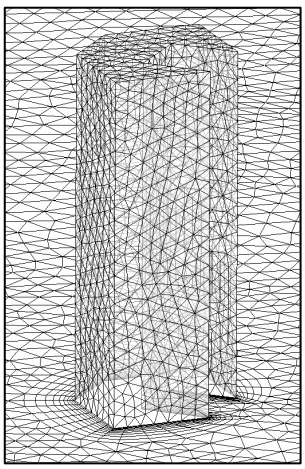

(a) Diamond C-Shape Model

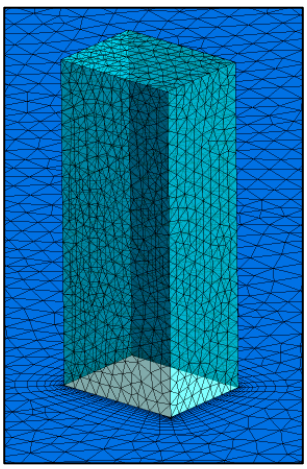

(b) Rectangular Model

Preprints (www.preprints.org) | NOT PEER-REVIEWED | Posted: 8 October 2023 doi:10.20944/preprints202310.0443.v1

Figure 5. Meshing Detail.

7. Flow Parameters and Boundary Conditions

Homogeneous steady-state wind flow under ABL at the inlet of the domain was provided with α = 0.143. Free stream velocity at the roof of the model attained was found to be 0.63 m/s. This velocity is sufficient to achieve critical R_e for turbulent flow around sharp-edged models like the present one. Figure 4 shows the velocity profile at the inlet. Free slip wall condition was provided on the domain side walls and top wall. The top of the model was also provided with free slip wall condition. By providing this condition it was ensured that flow parallel to the walls is free from frictional forces and is computable during the simulation. No slip wall condition was provided on the model surfaces and the ground of the domain to ensure that velocity at the surface is zero for making of boundary layer flow from the wall surfaces. To change the direction of the wind in a clockwise direction, the model is rotated in an anticlockwise direction with the same flow parameters and boundary conditions.

8. Result and discussion

8.1. Flow Pattern

For unconventional building plan shapes it is not guaranteed that the critical coefficient of pressure on faces shall be in the orthogonal direction of wind flow. Variation in pressure on the surfaces of any obstacle encountered by wind is influenced by wind flow patterns. Other mechanism associated with the wind flow pattern, such as vortex generation, drag and uplift forces, local eddies and turbulences, formation of a shear layer on surfaces, interference effects, etc. also influences the coefficient of pressure. In the present paper the values of surface pressures generated on the recessed faces D1, D2 & E of the model were evaluated to calculate the external mean coefficient of pressure (C_{Pe}) at wind incident angles 0°, 30°, 60°, 105°, 135° & 180°. On these wind angles critical values were plotted in the graph of area average C_{Pe} values on recessed faces (Figure 6). It is seen that the critical average suction pressure coefficient on the recessed faces D1, D2 & E are encountered on different angles of attack (AoA). The value of negative pressure on the faces is almost similar to 30° AoA. From 30° to 60° they go on increasing marginally. From the AoA 60° onwards the values are increasing substantially up to 105° AoA. However, the rate of increase of C_{Pe} on face D2 is more prominent than that on face D1. From there the value of negative pressure on faces is improving constantly and coming to nil in between 120° & 135° AoA. From there they change the sign and increase up to the AoA of 180°.

Figure 7 (a) to (f) shows the pattern of wind flow for wind incident angles 0°, 30°, 60°, 105°, 135° & 180°. Within the recessed well for the obliqued angle of flow it is found that the flow is separated from the frontal corner and a shear layer is formed. The separated shear layer is rolling up and is evolving vortices. Instability associated with the laminar-turbulent transition to turbulent flow on the suction side is seen creating vortices. The separated vortices are continuously hitting on the recessed surfaces. Creation of different wake and vortex on the leeward side, vortex & eddies within the opening/well of the recessed portion, separation of flow pattern from the side's faces and edges, and the impact of wind on the windward side is different for different wind angles.

Preprints (www.preprints.org) | NOT PEER-REVIEWED | Posted: 8 October 2023 doi:10.20944/preprints202310.0443.v1

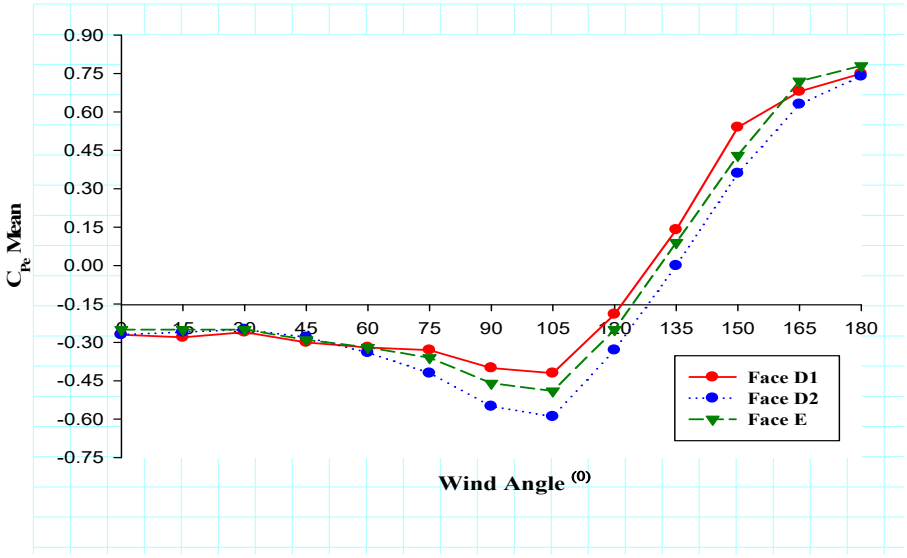

Figure 6. Variation of Mean CPe Values on Recessed Faces.

Figure 8 (a) to (f) shows the wind pattern along the wind direction on a vertical plane passing through the global origin of the model. The upwind ground vortex is different for different wind angles. It is also observed that the peak velocity differs for some wind incident angles. As Such, unlike the case of a regular shape model of the same height and plan area, the coefficient of pressure on surfaces of a diamond C-shaped model is expected to be different. Especially, on the faces of the recessed portion i.e., Face D1, D2, and E due to the interference effect among them.

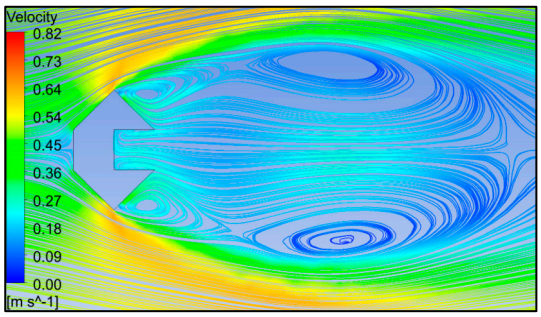

Figure 7 (a): 0° AoA

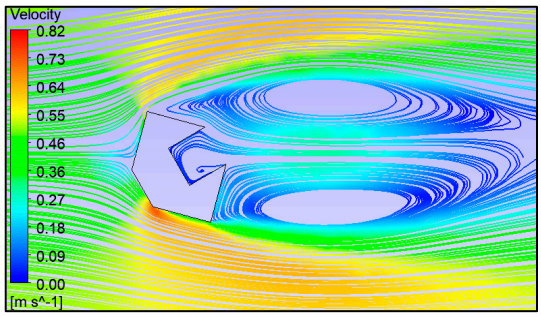

Figure 7 (b): 30° AoA.

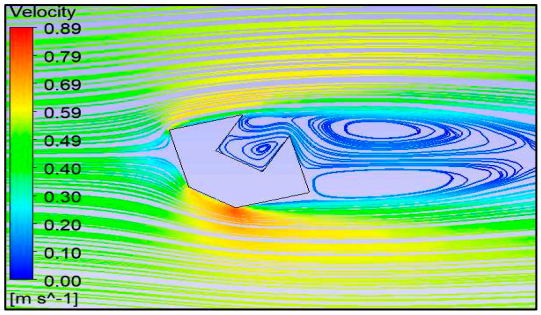

Figure 7 (c): 60° AoA

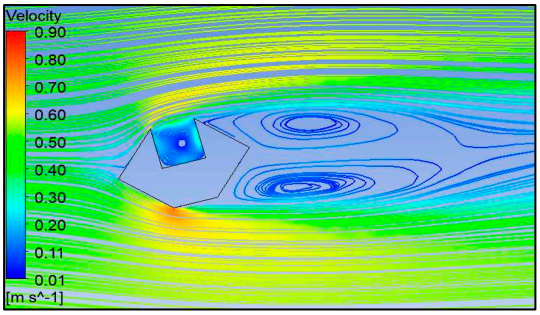

Figure 7 (d): 105° AoA.

Preprints (www.preprints.org) | NOT PEER-REVIEWED | Posted: 8 October 2023 doi:10.20944/preprints202310.0443.v1

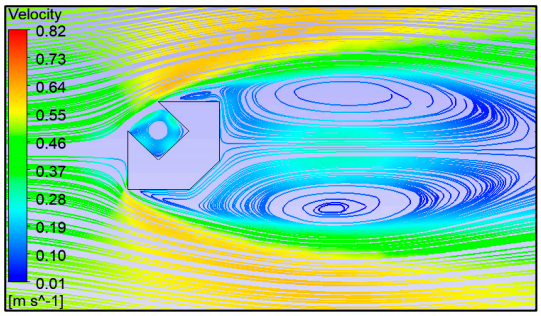

Figure 7 (e): 135° AoA

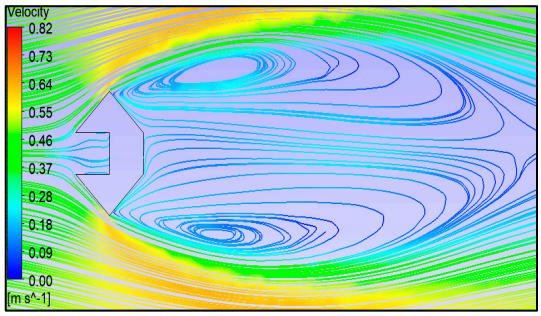

Figure 7 (f): 180° AoA.

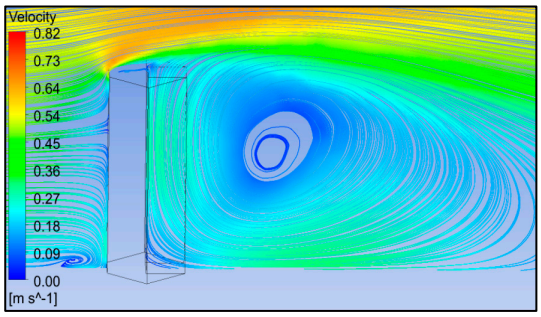

Figure 8 (a): 0°AoA

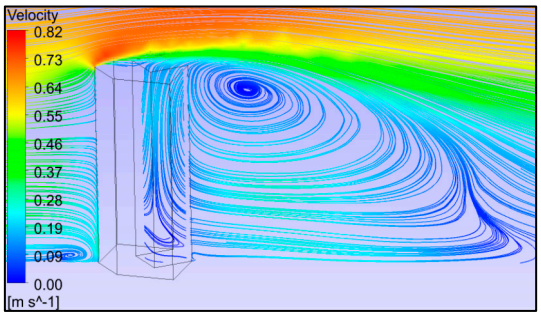

Figure 8 (b): 30° AoA

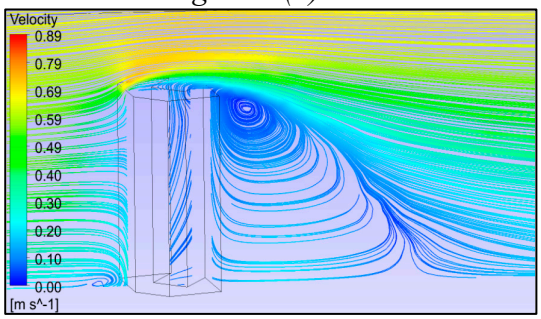

Figure 8 (c): 60° AoA

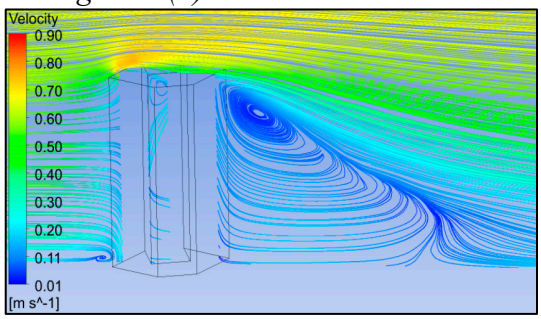

Figure 8 (d): 105° AoA

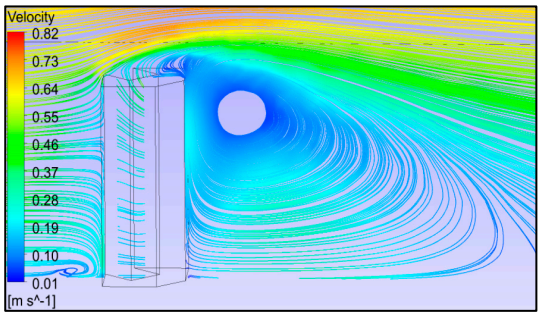

Figure 8 (e): 135° AoA

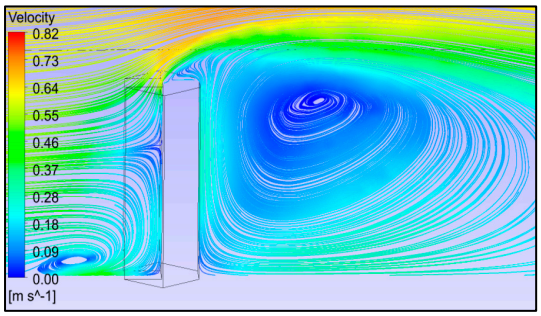

Figure 8 (f): 180° AoA

Figure 8. Wind Flow Pattern -Plan.

8.2. Pressure Coefficient on Faces

The C_{Pe} contours on recessed faces for 0°, 30°, 60°, 105°, 135° & 180° are presented in Figure 9 (a) to (f). Dissipation of wind energy by the incident wind on the windward face is found to cause positive pressure on the faces, whereas suction pressure on faces occurs due to vortex generation and uplift force created by backwash and/or sidewash. Figure 9 (f) shows that face E, which is the windward face for 180° AoA, is subjected to the highest positive pressure. The C_{Pe} value is almost constant throughout the width of the faces up to the height of almost the rooftop of the model. The mean C_{Pe} value on the

Preprints (www.preprints.org) | NOT PEER-REVIEWED | Posted: 8 October 2023 doi:10.20944/preprints202310.0443.v1

face is 0.78. Since the wind is entrapped and no flow separation from edges of face E is taking place, except the rooftop, the C_{Pe} is almost constant on the face except nearer to the rooftop. The wind after impact on face E is reflecting and indulges with limb faces D1 & D2 creating an interference effect on them. After a height of 0.4 m C_{Pe} is reducing rapidly, Figure 10 (f), and becomes negative before it touches the rooftop where the separation of flow and the uplift force increases velocity. The recessed limb faces parallel to the wind flow, D1 and D2, are also experiencing positive pressure of constant nature throughout their widths as the wind is entrapped after hitting face E, and reflecting on faces D1 and D2. The mean C_{Pe} on the faces D1 and D2 are 0.74/0.75. For 0^0 AoA, Figure 11 (a), the value of mean suction pressures on all three faces increases up to a height between 0.3 and then again progressively decreases towards the rooftop. Concentration points of pressure are also seen on some faces. This is due to the fact that the two-dimensional structure of the shear layer changes into the three-dimensional structure by vortex instability.

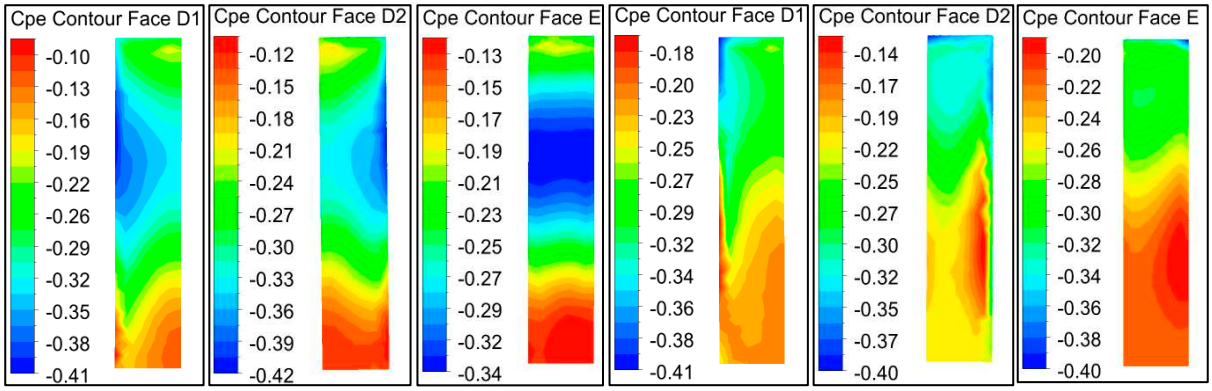

Figure 9 (a): C_{Pe} Contour 0° AoA *Figure 9 (b): C_{Pe} Contour 30° AoA*

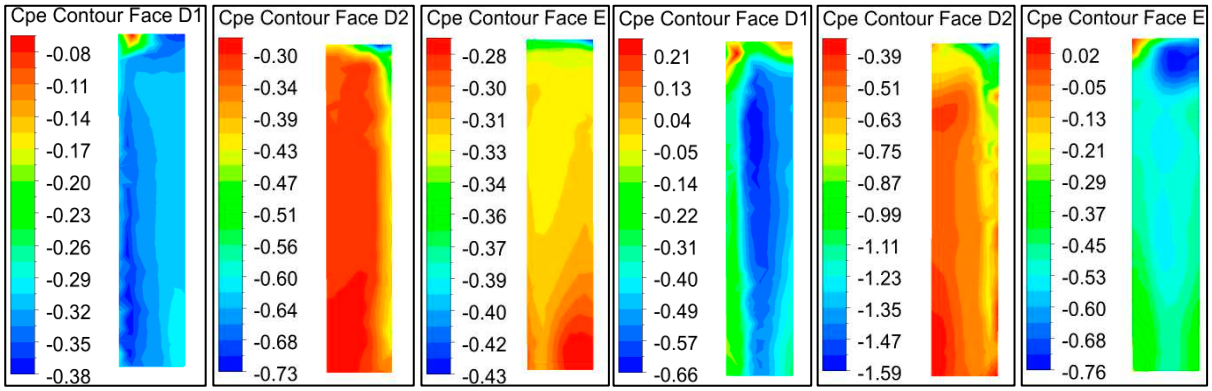

Figure 9 (c): C_{Pe} Contour 60° AoA *Figure 9 (d): C_{Pe} Contour 105° AoA*

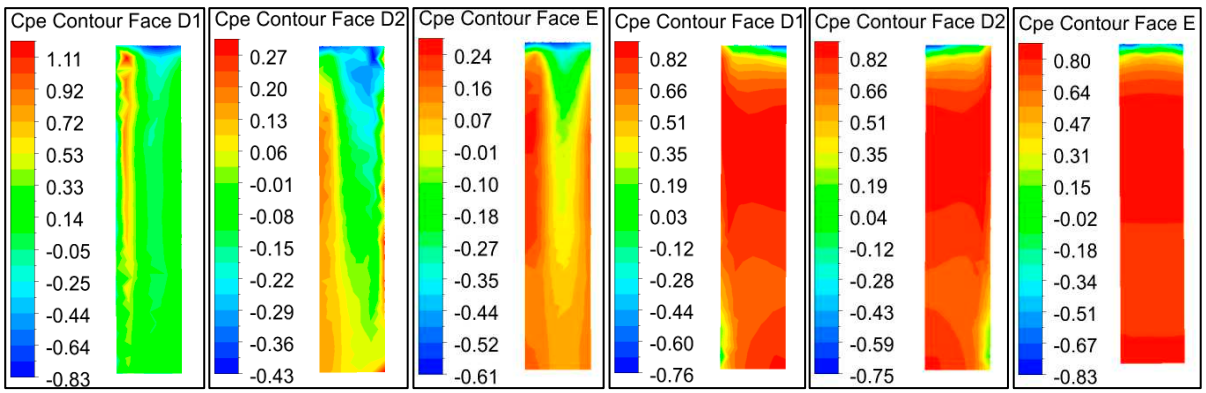

Figure 9 (e): C_{Pe} Contour 135° AoA *Figure 9 (f): C_{Pe} Contour 180° AoA*

Preprints (www.preprints.org) | NOT PEER-REVIEWED | Posted: 8 October 2023 doi:10.20944/preprints202310.0443.v1

Figure 9. Wind Flow Pattern -Elevation on a Central Vertical Plane.

8.3. Pressure Along Central Vertical Line.

Such plots provide us a realistic and fine picture of the pattern of pressure coefficients along the height of the faces and changes in flow pattern along the height can also be understood from them. The central vertical pressure on faces is shown in Figure 10 (a) to (f). Positive pressure along the central vertical line on the model surfaces is positive where the faces are obstructing the flow. At 0° wind angle, the recessed faces facing suction follow the same path along the vertical line and overlap with one another. The suction increases up to the height of 0.3 m and then decreases due to greater uplift force. As the wind incident angle changes, the central vertical C_{Pe} value on all the three faces are becoming straighter i.e., the C_{Pe} values are uniform. At a 60° wind angle, they are almost straight. Up to 105° wind angles, C_{Pe} values are negative. At 135° wind angle, the values are positive up to the height of 0.2 m and then grow to negative due to the channelizing effect along the height of the recessed well cavity. On face D1 fluctuations in the central vertical C_{Pe} is seen due to instability of microlevel turbulence and eddies created on the face. The C_{Pe} values on the faces are positive for 180° AoA and overlap with one another.

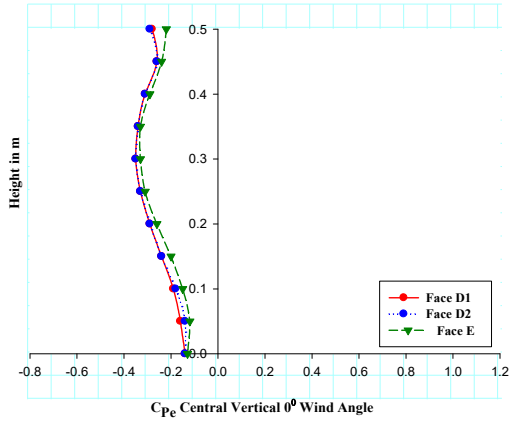

Figure 10 (a): Central Vertical C_{Pe} 0° AoA

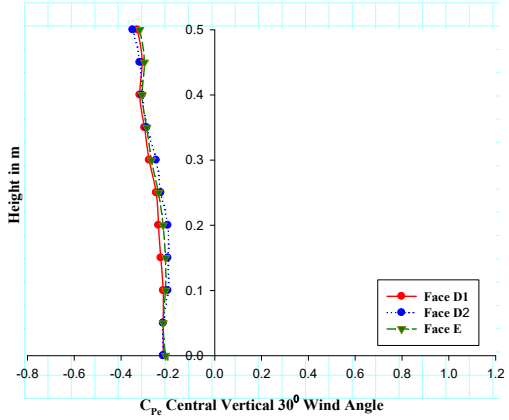

Figure 10 (b): Central Vertical C_{Pe} 30° AoA

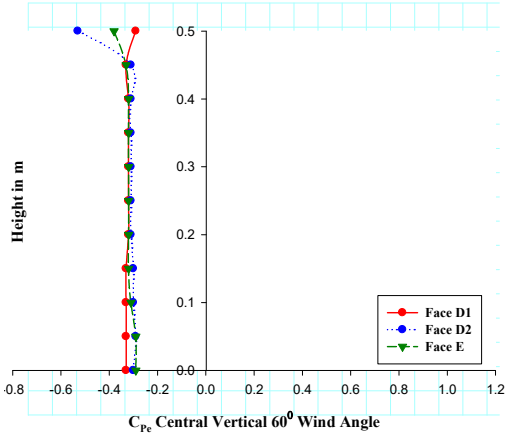

Figure 10 (c): Central Vertical C_{Pe} 60° AoA

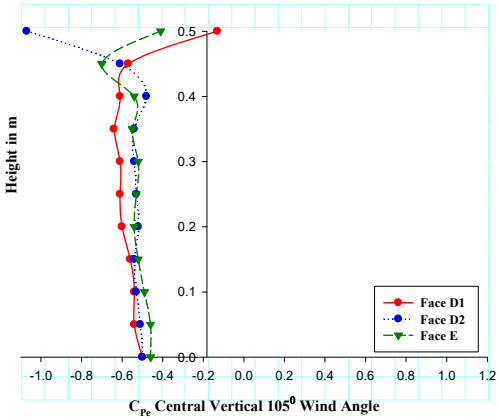

Figure 10 (d): Central Vertical C_{Pe} 105° AoA

Preprints (www.preprints.org) | NOT PEER-REVIEWED | Posted: 8 October 2023 doi:10.20944/preprints202310.0443.v1

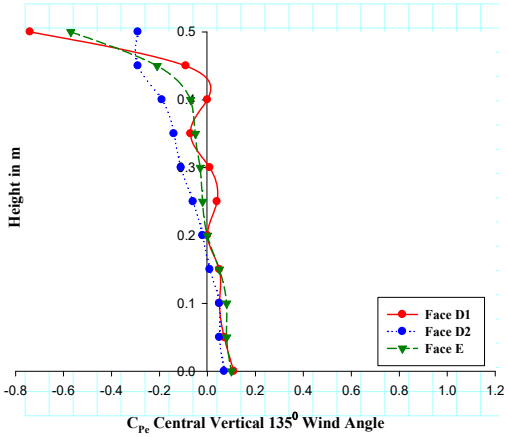

Figure 10 (e): Central Vertical C_{Pe} 135° AoA

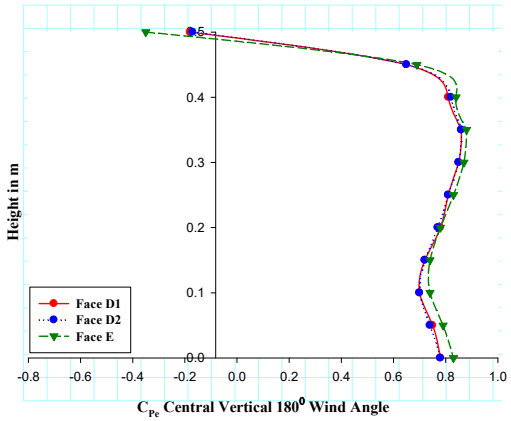

Figure 10 (f): Central Vertical C_{Pe} 180° AoA

8.4. Comparative Study of C_{Pe} Values

A comparative study of average C_{Pe} values on the recessed faces D1, D2 & E is shown in Figure 11. It is seen that for 0° & 180° AoA, the coefficient of pressure on faces D1 and D2 are almost symmetrical as the flow pattern within the recessed well is symmetrical. The mean coefficient of pressure on the faces is also shown. The values change sign at 135° AoA with the minimum numerical values on all three faces D1 (0.14), D2 (0.00) and E (0.09). At 60° AoA all the three faces have almost equal average C_{Pe} values D1 (-0.32), D2 (-0.34) & E (-0.32). The maximum suction occurs at 105° AoA on faces. It is -0.42 on face D1, -0.59 on face D2 and -0.49 on face E. So, a detailed investigation at different wind angles for unconventional plan shape buildings is a must on a case-to-case basis so that correct values may be incorporated during the design of cladding/glazing units.

9. Conclusion

The wind pressure data reported here is useful for identifying wind pressure distribution on the recessed sides of a C-plan diamond-shaped building. The present study has shown prominent output related to pressure (C_{Pe}) distributions on the recessed faces that can be induced due to changes in wind incidence angle. Suction pressure in the recessed side for different wind incidence angles is discussed and it is observed to be almost constant for less than 60° wind angle as flow tends to skip past the recess gap leaving stagnant flow in the recessed cavity. The recessed faces are subjected to a uniform pressure field at a 60° wind incidence angle. Due to changes in the angle of wind incidence, the increased pressure field turns out to be positive and the minimum positive value of the mean coefficient of pressure on the faces is found to be at 135° wind incidence angle.

Wind flow patterns from ANSYS (CFX) based on the standard $k-\varepsilon$ turbulent model provide us a good idea of the modification of wind flow around the bluff body. However, the quality of numerical results can be improved by making different meshing grid arrangements in various regions of flow as per expected turbulent characteristics in the region. Nevertheless, the results obtained can provide useful information about wind pressure distributions on such irregular plan shapes.

Preprints (www.preprints.org) | NOT PEER-REVIEWED | Posted: 8 October 2023 doi:10.20944/preprints202310.0443.v1

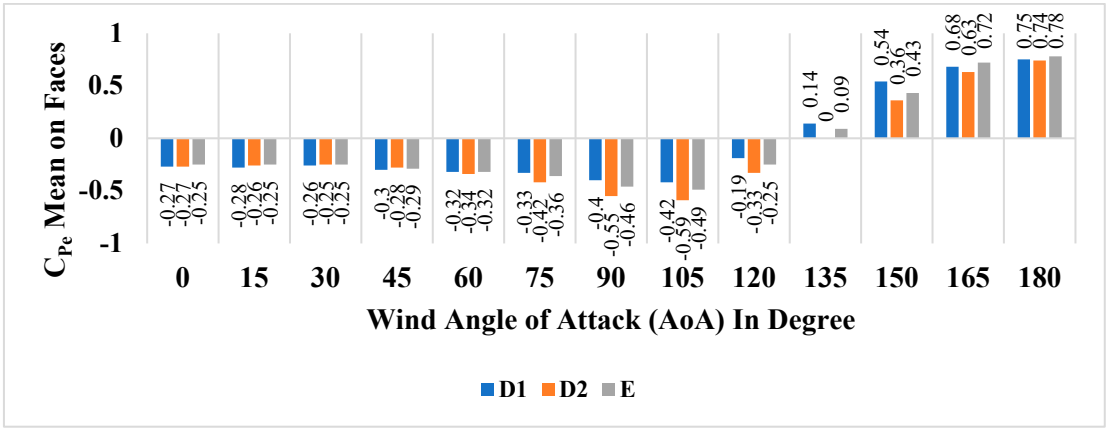

Figure 11. Comparative Study of C_{Pe} on Faces for Different AoA.

Author Contributions: Conceptualization, A.K., and R.K.M.; Methodology, A.K., R.K.M. and R.R.; Software, A.K., R.K.M. and R.R.; Validation, R.R., M.I.K. and J.M.K; Formal analysis, A.K. and R.K.M.; Resources, M.I.K and J.M.K.; Writing – original draft, A.K.; Writing – review & editing, R.R., R.K.M., M.I.K. and J.M.K; Supervision, R.R. All authors have read and agreed to the published version of the manuscript.

Funding: The authors extend their appreciation to Researcher Supporting Project number (RSPD2023R692), King Saud University, Riyadh, Kingdom of Saudi Arabia.

Institutional Review Board Statement: Not applicable.

Informed Consent Statement: Not applicable.

Data Availability Statement: Not applicable.

Acknowledgments: The authors extend their appreciation to Researcher Supporting Project number (RSPD2023R692), King Saud University, Riyadh, Kingdom of Saudi Arabia.

Conflicts of Interest: The authors declare no conflict of interest.

References

1. R. K. Pradeep, V. Ehsan, and S. Azadeh, "Computation Fluid Dynamics Approach for Highrise Buildings," *Centre for Earthquake Engineering, IIIT Hyderabad, A3C-12, Report No. IIIT/TR/2013/-1*, Hyderabad, pp. 1–9, 2013.
2. H. L. Dryden and G. C. Hill, "Wind Pressure on Structures," *Scientific Papers of the Bureau of Standards*, pp. 698–732, Oct. 1925.
3. J. D. Holmes, *Wind Loading of Structures*, Third Edition. CRC Press, 2015.
4. Taranath Bungale S., *Wind And Earthquake Resistant Buildings*. New York: Marcel Dekker, 2004.
5. W. D. Baines, "Effect of Velocity Distribution on Wind Loads on a Tall Building," 1952.
6. M. G. Gomes, A. Moret Rodrigues, and P. Mendes, "Experimental and numerical study of wind pressures on irregular-plan shapes," *Journal of Wind Engineering and Industrial Aerodynamics*, vol. 93, no. 10, pp. 741–756, 2005, doi: 10.1016/j.jweia.2005.08.008.
7. C. Chor Kwan Cheng, K. Ming Lam, A. Leung, C. C. Cheng, K. Lam, and A. Y. Leung, "Wind flow in the recessed cavities of a tall building," 2009. [Online]. Available: https://www.researchgate.net/publication/255566643
8. Z. Xu and J. Yin, "The Influence of Aeroelastic Effects on Wind Load and Wind-Induced Response of a Super-Tall Building: An Experimental Study," *Buildings*, vol. 13, no. 7, 2023, doi: 10.3390/buildings13071871.
9. J. A. Amin and A. K. Ahuja, "Experimental study of wind-induced pressures on buildings of various geometries," 2011. [Online]. Available: www.ijest-ng.com
10. J. A. Amin and A. K. Ahuja, "Mean interference effects between two buildings: Effects of close proximity," *Structural Design of Tall and Special Buildings*, vol. 20, no. 7, pp. 832–852, Nov. 2011, doi: 10.1002/tal.564.
11. Tanaka H, Tamura Y, Ohtake K, Nakai M, Kim YC, and Bandi E K, "Experimental Investigation of Aerodynamic Forces and Wind Pressure Acting on Tall Buildings with Various Unconventional Configuration," *Journal of Wind Engineering and Industrial Aerodynamics*, vol. 107–108, pp. 179–191, 2013.
12. S. Zhao, C. Zhang, X. Dai, and Z. Yan, "Review of Wind-Induced Effects Estimation through Nonlinear Analysis of Tall Buildings, High-Rise Structures, Flexible Bridges and Transmission Lines," *Buildings*, vol. 13, no. 8, pp. 1–24, 2023, doi: 10.3390/buildings13082033.

13. Kheyari P and Dalui S.K, "Estimation of Wind Load on a Tall Building Under Interference Effect," *Jordon J Civil Eng*, vol. 9, no. 1, pp. 84–101, 2014.
14. R. K. Meena, R. Raj, and S. Anbukumar, "Effect of wind load on irregular shape tall buildings having different corner configuration," *Sadhana - Academy Proceedings in Engineering Sciences*, vol. 47, no. 3, 2022, doi: 10.1007/s12046-022-01895-2.
15. R. Kar and S. K. Dalui, "Wind interference effect on an octagonal plan shaped tall building due to square plan shaped tall buildings," *International Journal of Advanced Structural Engineering (IJASE)*, vol. 8, no. 1, pp. 73–86, 2016, doi: 10.1007/s40091-016-0115-z.
16. S. Charisi, T. K. Thiis, and T. Aurlien, "Full-scale measurements of wind-pressure coefficients in twin medium-rise buildings," *Buildings*, vol. 9, no. 3, 2019, doi: 10.3390/buildings9030063.
17. X. L. Bowen Yan, Yanan Li and Q. Y. and X. Z. , Xuhong Zhou, Min Wei, "Wind Tunnel Investigation of Twisted Wind Effect on a Typical," 2022.
18. A. Kumar Bairagi and K. Dalui, "COMPARISON OF PRESSURE COEFFICIENT BETWEEN SQUARE AND SETBACK TALL BUILDING DUE TO WIND LOAD," in *11th Structural Engineering Convention* , 2018, pp. 1–6. [Online]. Available: https://www.researchgate.net/publication/329786479
19. B. Bhattacharyya and S. K. Dalui, "Investigation of mean wind pressures on 'E' plan shaped tall building," *Wind and Structures, An International Journal*, vol. 26, no. 2, pp. 99–114, Feb. 2018, doi: 10.12989/was.2018.26.2.099.
20. S. K. Nagar, R. Raj, and N. Dev, "Experimental study of wind-induced pressures on tall buildings of different shapes," *Wind and Structure*, vol. 31, no. 5, pp. 441–453, 2020.
21. S. Kumar Nagar, R. Raj, and N. Dev, "Proximity effects between two plus-plan shaped high-rise buildings on mean and RMS pressure coefficients," *Scientia Iranica*, pp. 1–28, 2021.
22. H. Pan, J. Wu, and J. Fu, "Monitoring of Wind Effects on a Super-Tall Building under a Typhoon," *Buildings*, vol. 13, no. 1, 2023, doi: 10.3390/buildings13010047.
23. M. Mallick, A. Mohanta, A. Kumar, and V. Raj, "Modelling of Wind Pressure Coefficients on C-Shaped Building Models," *Modelling and Simulation in Engineering*, vol. 2018, pp. 1–13, 2018, doi: 10.1155/2018/6524945.
24. J. A. Amin and A. K. Ahuja, "Effects of Side Ratio on Wind-Induced Pressure Distribution on Rectangular Buildings," *Journal of Structures*, vol. 2013, pp. 1–12, Aug. 2013, doi: 10.1155/2013/176739.
25. ANSYS Inc, *ANSYS CFX-Solver Theory Guide*. 2009. [Online]. Available: http://www.ansys.com
26. Revuz J, Hargeaves D. M, and Owen J.S., "On the Domain Size for the Steady State CFD Modeling of a Tall Building," *Wind Structure*, vol. 15, no. 4, pp. 313–329, 2012.